Pergamon

Bioorganic & Medicinal Chemistry 6 (1998) 1799–1810

BIOORGANIC & MEDICINAL CHEMISTRY

Structure-based Design and Synthesis of Small Molecule Protein–Tyrosine Phosphatase 1B Inhibitors†

Zhu-Jun Yao,[a] Bin Ye,[a] Xiong-Wu Wu,[b] Shaomeng Wang,[b] Li Wu,[c] Zhong-Yin Zhang[c] and Terrence R. Burke, Jr.[a,*]

[a]*Laboratory of Medicinal Chemistry, Division of Basic Sciences, National Cancer Institute, National Institutes of Health, Bethesda, MD 20892, USA*

[b]*Institute for Cognitive and Computational Sciences, Georgetown University Medical Center, Washington, DC 20007, USA*

[c]*Department of Molecular Pharmacology, Albert Einstein College of Medicine, Bronx, NY 10461, USA*

Received 19 March 1998; accepted 11 May 1998

Abstract—Protein–tyrosine phosphatase (PTP) inhibitors are attractive as potential signal transduction-directed therapeutics which may be useful in the treatment of a variety of diseases. We have previously reported the X-ray structure of 1,1-difluoro-1-(2-naphthalenyl)methyl] phosphonic acid (**4**) complexed with the human the protein–tyrosine phosphatase 1B (PTP1B) and its use in the design of an analogue which binds with higher affinity within the catalytic site (Burke, T. R., Jr. et al. *Biochemistry* **1996**, *35*, 15989). In the current study, new naphthyldifluoromethyl phosphonic acids were designed bearing acidic functionality intended to interact with the PTP1B Arg47, which is situated just outside the catalytic pocket. This residue has been shown previously to provide key interactions with acidic residues of phosphotyrosyl-containing peptide substrates. Consistent with trends predicted by molecular dynamics calculations, the new analogues bound with 7- to 14-fold higher affinity than the parent **4**, in principal validating the design rationale.

Introduction

Protein–tyrosine kinase (PTK) dependent signal transduction is achieved through modulating the phosphorylation states of tyrosyl residues (pTyr, **1**) in key cellular proteins. An imbalance in the PTK-mediated generation of phosphotyrosyl (pTyr) residues versus dephosphorylation by protein–tyrosine phosphatases (PTPs)[1–6] can contribute to a variety of diseases, making development of both PTK and PTP inhibitors of potential interest. While significant progress has been made in the preparation of PTK inhibitors,[7] considerably less has been reported in the PTP inhibitor field,[8] in spite of the attractiveness of these latter targets.

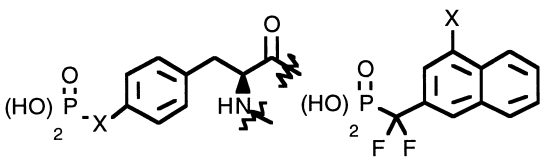

1 X = O pTyr **4** X = H

2 X = CF_2 F_2Pmp **5** X = OH

3 X = CH_2 Pmp

Utilizing the nonreceptor phosphatase PTP1B as a model, we have approached PTP inhibitor development by an iterative process of: (1) inhibitor design and synthesis; (2) biological evaluation/enzyme–ligand structure elucidation; and finally, (3) redesign, to progress from peptide-based inhibitors toward progressively more potent small molecule analogues. Exemplary is

Key words: Amino acids and derivatives; mimetics; phosphonic acids and derivatives; phosphorylation.

*Corresponding author. Tel.: (301) 402-1717; Fax: (301) 402-2275; E-mail: tburke@helix.nih.gov

†A preliminary account of this work have been reported: Burke, T. R., Jr.; Yao, Z. J.; Ye, B.; Wang, S.; Zhang, Z. Y. Structure-based design of protein–tyrosine phosphatase inhibitors. Presented at the 213th National ACS Meeting, San Francisco, CA, April 13–17, 1997; MEDI-313.

0968-0896/98/$—see front matter
PII: S0968-0896(98)00140-0

our initial discovery that replacement of the pTyr residue in the peptide substrate "D-A-D-E-pY-L"[9] with the hydrolytically stable pTyr analogue, difluorophosphonomethyl phenylalanine[10,11] (F_2Pmp, **2**), resulted in an extremely potent PTP1B inhibitor ($IC_{50} = 100\,\mu M$).[12] The importance of the difluorophosphonate moiety in PTP binding interactions was dramatically illustrated by the much reduced inhibitory potency of the corresponding peptide substituted with the nonfluorine-containing phosphonomethyl phenylalanine residue (Pmp, **3**; $IC_{50} = 200\,\mu M$). In subsequent studies we showed that simple aryldifluoromethyl phosphonates lacking peptide component, also retained reasonable inhibitory potency if a polycyclic ring system, such as naphthyl (for example [1,1-difluoro-1-(2-naphthalenyl)methyl] phosphonic acid **4**) was employed rather than the single phenyl ring found in pTyr or F_2Pmp.[13] In order to understand the structural basis for the binding of such polycyclic-containing difluorophosphonates, we have solved the X-ray structure of **4** complexed within the PTP1B catalytic site, and based on the observed binding interactions a new naphthyl analogue (**5**) was designed that contains a hydroxyl group which mimics H_2O molecules originally bound within the PTP1B·**4** catalytic site. This modification resulted in a twofold increase in inhibitory potency of **5** relative to parent **4**, thereby supporting the principle of structure-based design as a means of increasing inhibitory potency.[14]

While these previous studies focused on enzyme inhibitor interactions within the pTyr binding cavity, it became of equal interest to examine potential interactions outside the actual catalytic site. It is recognized that in small pTyr-containing substrates, acidic residues proximal to the pTyr residue enhance binding affinity.[15] A structural basis for this empirical observation became evident from the X-ray structure of PTP1B complexed to the D-A-D-E-pY-L-amide hexapeptide, where it was seen that a critical arginine residue (Arg47) situated just external to the pTyr binding pocket, entered into key ionic interactions with the side chain carboxyl groups Glu and Asp residues situated in the pTyr-1 and pTyr-2 positions of the substrate peptide.[16] Based on the assumption that similar types of interactions with Arg47 could potentially be taken advantage of by small molecule inhibitors, the present study was undertaken to prepare new inhibitors of PTP1B using the structure of parent naphthyldifluoromethyl phosphonate **4**, which could potentially interact with Arg47.

Inhibitor design

The work by Jia et al.[16] highlighted the favorable binding interactions of the "E-pY" portion of the larger D-A-D-E-pY-L-amide peptide, in which the pTyr residue bound within the catalytic site and the Glu residue bound to Arg47 at the lip of the pTyr binding pocket. Using this in conjunction with our finding that F_2Pmp serves as a very potent pTyr mimetic in the context of PTP inhibitors, and that naphthyl-containing difluoromethyl phosphonates can also bind with good affinity, we sought to prepare small molecule inhibitors based on the "Ac-E-pY-amide" structure (**6**), in which either F_2Pmp or naphthyldifluoromethyl phosphonic acid moiety **4** served as pTyr replacements. When using F_2Pmp as a pTyr replacement, dipeptide **7** resulted in a straight forward fashion. For naphthyl-based analogues using **4** as a pTyr replacement, it was less obvious how the parent **4** should be modified in order to allow attachment of the Glu residue. The most direct approach was to add a carboxyl group at the naphthyl 6-position to yield analogue **9**, which was reminiscent of a ring-constrained version of F_2Pmp. However, since compound **9** lacked critical α-amino functionality found in the parent F_2Pmp, coupling of **9** with a Glu residue could not occur in a manner directly analogous to that seen in parent dipeptide **7**. Instead the "pseudodipeptide" **10** would result, in which the Glu residue effectively becomes situated at the carboxyl-terminal side of the construct, similar to the "reverse order" dipeptide **8**. The effects of this were unclear, since the differential importance of residues situated amino versus carboxyl terminal to the pTyr residue had previously been shown for small phosphopeptide substrates.[9] Additionally, the original structural interaction of the Glu residue of the parent D-A-D-E-pY-L peptide with Arg47 of the PTP1B complex, was based on its location to the amino side of the pTyr residue.[16] Further adding to the uncertainty of analogue **9**, was that when viewed as a pTyr mimetic, the embedded phenylpropanoyl side chain was effectively constrained to coplanarity, while in the actual PTP1B-bound peptide, the side chain of the pTyr residue projected at an angle nearly perpendicular to the plane of the phenyl ring.[16] Because of these ambiguities in the manner in which **10** would mimic parent **7**, we also designed the isomeric naphthyl-containing dipeptide mimetic **11**. While **11** effectively places the difluorophosphonate group in the wrong position relative to parent F_2Pmp-containing **7**, our previous studies had demonstrated that significant latitude is permitted in the placement of the difluorophosphonate group relative to the naphthyl ring.[13,14] In light of these considerations, it also seemed appropriate to prepare the sequence-reversed dipeptide **8** for purposes of comparison.

Synthesis

Central to the synthesis of target dipeptide mimetics **10** and **11** was the regiochemically controlled introduction of carboxylate functionality onto the parent (di-*tert*-butyl) (2-difluoromethyl)naphthyl phosphonate structure. For **10** and **11**, this required carboxylation at the 6-

and 7-positions of the naphthyl ring, respectively. Our initial approach toward the synthesis of bis(*tert*-butyl) aryl(difluoromethyl)phosphonates involved diethylaminosulfur trifluoride (DAST)-mediated fluorination of the corresponding ketophosphonates, which themselves were obtained by addition of (di-*tert*-butyl)phosphite to the aryl aldehydes, followed by oxidation of the resulting α-hydroxyphosphonates.[17] Although ketophosphonates have also been prepared by addition of phosphites to acyl chlorides, we have been unsuccessful at preparing *tert*-butyl-protected ketophosphonates by this more direct route. Recently, a number of new approaches toward the synthesis of aryl(difluoromethyl)phosphonates have appeared which do not rely on intermediate ketophosphonates,[18,19] including the preparation of naphthyl bis[(difluoromethyl)phosphonates].[20] However, none of these reported synthesis provided *tert*-butyl-protected phosphonates, which we desired in order to allow facile cleavage of phosphonate protection under mild acidic conditions. Based on these considerations, we decided to utilize our original ketophosphonate-route.

Our synthesis of dipeptide mimetics **10** and **11** relied on the preparation of naphthoic acids **19** and **33**, respectively, which would subsequently be coupled under solid-phase protocol to resin-bound Glu residues (Schemes 1 and 2). For synthesis of **19** and **33** by our ketophosphonate approach, aldehydes **15** (Scheme 1) and **29** (Scheme 2) became intermediate targets. Both **15** and **29** were prepared by oxidation of benzylic alcohols. In the case of aldehyde **15**, commercially available 2,6-naphthalenedicarboxylic acid **12** was first differentially protected as the monobenzylic ester **13** and then reduced to the corresponding benzylic alcohol **14**, which upon oxidation, yielded aldehyde **15**. A somewhat more lengthy route was utilized to obtain aldehyde **29**.

Carboxymethylation of commercially available 2,7-dihydroxynaphthalene **20** was preceded by its activation as the bistriflate **21** followed by exposure to carbon monoxide under the catalysis of $Pd(OAc)_2$ in the presence of $Ph_2P(CH_2)_3PPh_2$. Mono-deprotection of the resulting 2,7-dicarbomethoxynaphthalene **22**, which would be required to differentiate the two benzylic positions, was not readily achieved. However, after reduction to diol **23** ($LiAlH_4$), selective silation of a single alcohol was possible, providing monobenzylic alcohol **24**. This selective silation was achieved using TBDMSCl and $LiN(SiMe_3)_2$ in THF, but not using TBDMSCl and imidazole in DMF. Conversion of alcohol **24** to benzyl ester **27** was done in a two-step fashion through aldehyde **25** (oxidation using MnO_2) and carboxylic acid **26** (treatment with buffered $NaClO_2$) followed by alkylation with benzyl bromide (DBU in DMF). Finally, removal of silyl protection (tetrabutylammonium-

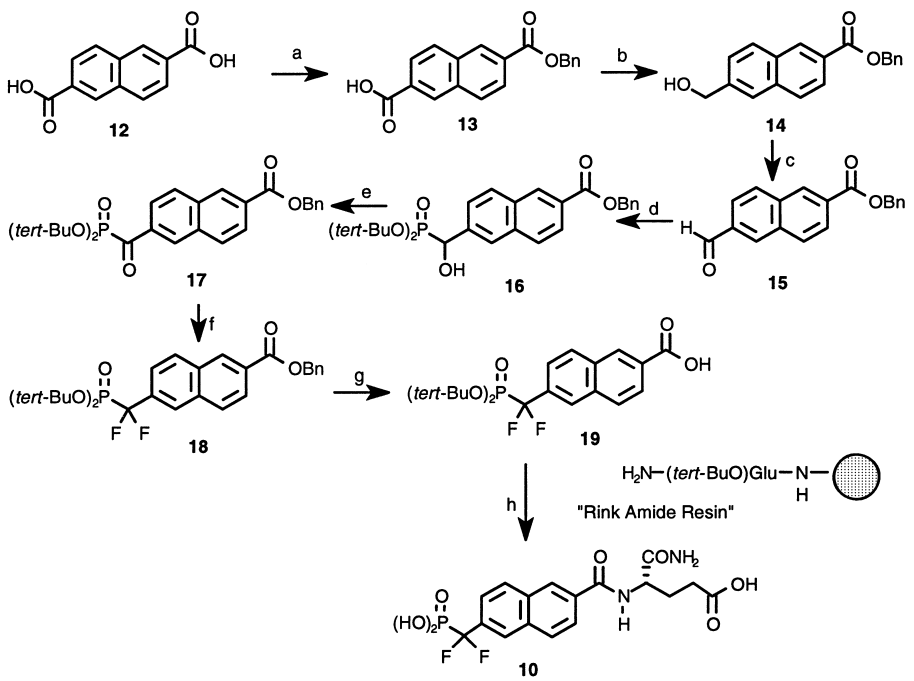

Scheme 1. Reagents and conditions: (a) DBU, BnBr, DMF, 17%; (b) BH_3·THF, THF, 84%; (c) MnO_2, toluene, 100%; (d) $(^tBuO)_2P(O)H$, basic Al_2O_3, 91%; (e) Swern oxidation; (f) DAST, 59%; (g) 0.2 N LiOH, THF, 74%; (h) DIPCDI, HOBt, NMP; then TFA, anisole; HPLC, 44%.

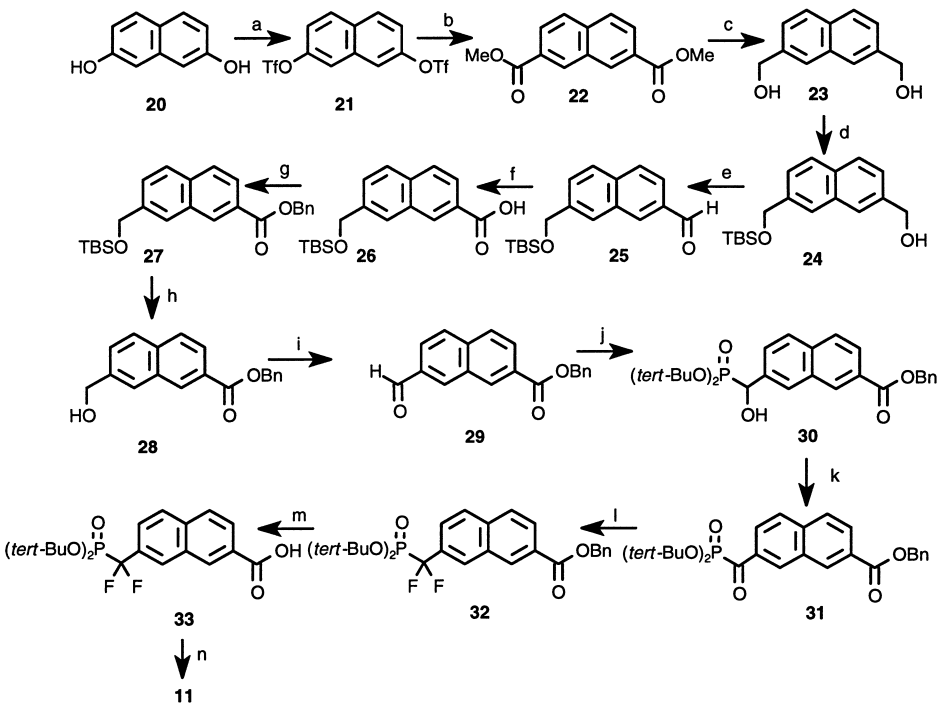

Scheme 2. Reagents and conditions: (a) Tf_2O, 2,6-lutidine, DMAP, CH_2Cl_2-THF, 74%; (b) $Pd(OAc)_2$, dppp, CO, MeOH, TEA, DMSO, 84%; (c) LiAlH4, THF, 59%; (d) LiHMDS, TBDMSCl, 45%; (e) MnO_2, toluene, 77%; (f) NaClO2, KH_2PO_4, 2-methyl-2-butene, ^{t}BuOH–water, 98%; (g) DBU, BnBr, DMF, 92%; (h) TBAF, THF, 93%; (i) PCC, CH_2Cl_2, 95%; (j) (^{t}BuO)$_2$P(O)H, LiHMDS, THF, 98%; (k) Swern oxidation, 71%; (l) DAST, 52%; (m) 0.2 N LiOH, THF; (n) DIPCDI, HOBt, NMP; TFA, anisole; HPLC, 30%.

fluoride) and oxidation (PCC) of the resulting benzylic alcohol **28** gave desired aldehyde **29**.

Isomeric aldehydes **15** and **29** were converted to *tert*-butyl protected difluorophosphonates **18** and **33** respectively, according to our published three-step procedure.[17] Synthesis of dipeptide mimetics **10** and **11** were then achieved by HOBT active ester solid-phase techniques using (O^{γ}-*tert*-butyl)glutamic acid attached to a Rink amide resin.[21] The importance of *tert*-butyl protection was then demonstrated, as treatment with TFA resulted in concomitant cleavage from the resin and removal of all protecting groups. Synthesis of F_2Pmp-containing dipeptides **10** and **11** was also achieved by solid-phase techniques using Rink amide resin and N^{α}-Fmoc F_2Pmp which lacked phosphonate protection.[22]

Results and Discussion

Molecular modelling

To demonstrate the validity of our stepwise protocol, molecular dynamics simulations were performed on the X-ray structures of PTP1B in complex alternatively with **4**[14] and the tetrapeptide "Ac-D-E-pY-L" (**35**).[16] In both cases, significant conformational and energetic changes were observed at higher temperatures ($T > 298$ K), however at room temperature ($T = 298$ K) structures remained in low energy conformations throughout the simulation intervals. Final trajectories were very close to the actual X-ray structures in both cases, with root-mean-square (RMS) values for all atoms being $1.03\approx$ and $1.09\approx$ for complexes involving **4** and **35**, respectively. The most significant conformational differences arose from the phosphate-binding loop region. All molecular dynamics simulations were conducted using a stepwise protocol rather than at constant temperature. In this fashion, local energy barriers were more readily overcome, resulting in lower energy enzyme–inhibitor complexes (see Experimental section). This was shown by comparing results of stepwise dynamics simulations with those obtained at constant temperature. For the complex PTP1B·**4** after 100 ps of simulation at a constant temperature of 298 K, an average potential energy of -9974 kcal mol^{-1} for final trajectories, was 203 kcal mol^{-1} higher than the corresponding value of $-10{,}077$ kcal mol^{-1} obtained by a stepwise simulation. Similar potential energy differences were observed for the complex PTP1B·**35**, indicating that the stepwise

simulation is more effective in delineating low energy conformations, and this protocol was therefore employed for all systems in the present study.

As previously described, naphthyl dipeptide mimetics **10** and **11** were designed empirically based on observed favorable "E-pY" interactions in the X-ray structure of a PTP1B-bound phosphopeptide.[16] Once designed, the ability of these analogues to interact both within the pTyr binding pocket and with external elements outside the pocket, noteably the Arg47 residue, were evaluated by molecular dynamics simulations. Dynamics simulations of the complex PTP1B·**10** resulted in phosphonate, difluoromethylene, and naphthyl ring orientations assuming orientations quite similar to those observed for the parent complex PTP1B·**4**. In both cases, the phosphonate oxygens all form strong hydrogen bonds to the protein, with one oxygen bonding to the backbone amide hydrogens of Ser216 and Ala217. A second oxygen forms two hydrogen bonds with backbone amide hydrogen and the side chain guanidino group of Arg221. This oxygen also forms a third hydrogen bond to the side chain hydroxyl of Ser215. The third phosphonate oxygen hydrogen bonds to the backbone amides of Gly218, Ile219, and Gly220, while the two geminal fluorine atoms hydrogen bond to the backbone amido group of Phe182 and the side chain carboxamide of Gln266. The naphthyl ring of **10** is sandwiched between a number of hydrophobic residues, with Tyr46, Val49, Ala217, and Ile219 lying on one face and Phe182 situated in an oblique fashion on the opposite face.

Of special interest in the present study, were potential interactions between inhibitor functionality with residues outside the pTyr binding pocket, particularly with Arg47. By design, it was hoped that the side chain carboxyl of **10** would be able to interact with the positively charged guanidino group of the Arg47 residue. Molecular dynamics simulations indicated that while such interactions could occur readily, they were highly reversible in nature, with rapid on/off exchange occurring between guanidino, carboxyl and solvent. Such fluidity was not totally unexpected in a surface phenomena of this nature. In some tragetories of the dynamics simulation, binding of **10** occurred with its side chain carboxyl group interacting with water. At the same time, three hydrogen bonds formed between its terminal carboxamido group and the enzyme; one between its amido hydrogens and the side chain carboxyl group of Asp48 and one each between the carbonyl and the backbone amide groups of Asp48 and Val49. In other trajectories, the carboxyl group interacts directly with the Arg47 guanidino group. The appended carboxyl group of **10** also interacts well with the protein, forming one hydrogen bond with the backbone amido group of Arg47. Taken together, these newly introduced hydrogen bonds most probably contribute significantly to the higher binding affinity of **10** relative to parent **4**.

For the complex PTP1B·**11**, binding interactions of the phosphonate, difluoromethylene, and naphthyl rings are all quite similar to those observed for **4** and **10**, with major differences between **10** and **11** stemming from hydrogen bonding patterns of inhibitor side chain functionality. Similar to **10**, the side chain carboxyl group of **11** could enter into a hydrogen bond with the backbone amido group of Arg47, however unlike **10**, the terminal carboxamido group of **11** did not interact with the protein. The loss of these three potential hydrogen bonds could contribute significantly to the observed lower binding affinity of **11**.

Dynamics simulations of PTP1B complexes with tripeptides **7** and **8**, show that the phosphonate and difluoromethylene groups bind with the enzyme in fashions identical to those observed for **4**, **10**, and **11**. The phenyl rings of both **7** and **8** interact with the hydrophobic side chains of Val49 and Ala217. However, the Glu side chain carboxyl of **7** forms two hydrogen bonds to the side chain guanidino group of Arg47, while Glu carboxyl group of **8** forms only one such hydrogen bond. The C-terminal Glu carboxamido group of **7** hydrogen bonds with the side chain carboxyl of Asp48. In binding of naphthyl-based inhibitors **4, 10**, and **11**, the Tyr46 aryl ring is twisted by at least 30 degrees relative to that observed for peptide analogues **7, 8**, and **35**, in which flexible phenyl rings are present. Overall, the improved binding observed for inhibitors correlated well with formation of new hydrogen bonds, particularly in the loop region between Tyr46 to Val49.

Biological evaluation

The effect of the aryldifluromethylphosphonates on the PTP1B catalyzed *p*-nitrophenyl phosphate (*p*NPP) hydrolysis reaction was examined at 30 °C and pH 7. The small aryldifluromethylphosphonates examined in this study inhibited the PTP reaction and the mode of inhibition was competitive with respect to the substrate (data not shown). The K_i values are summarized in Table 1. There are several points that are worth discussing. We have previously found that F_2Pmp-containing peptides are potent inhibitors of PTP1B.[14,23] It has been suggested, based on the X-ray structure of a complex between PTP1B and a peptide substrate, that the recognition pocket for pTyr provides the dominant driving force for peptide substrate binding.[16] Thus, we thought that the aryldifluromethylphosphonate moiety might represent a good starting point for designing low molecular weight, nonpeptide PTP inhibitors. While the simplest aryldifluromethylphosphonate, α,α-difluorobenzyl phosphonic acid (**34**),[13,17] exhibited a K_i value of

only 2.5 mM, adding a second phenyl ring (compound **4**,[13,14] $K_i = 179\ \mu M$) enhanced the affinity 14-fold. This suggests that there is considerable plasticity in the pTyr binding pocket, and that appropriately positioned hydrophobic functionalities can improve the binding efficacy. Indeed, the structure of PTP1B complexed with **4** shows that the naphthalene ring forms specific hydrophobic interactions with side chains of active site residues.[14]

The affinity of α,α-difluorobenzyl phosphonic acid **34** is nearly 14,000-fold lower than Ac-D-A-D-E-F_2Pmp-L-amide ($K_i = 0.18\ \mu M$).[23] This result also implies that structural features in addition to the F_2Pmp motif are required for high affinity binding. Kinetic studies with

Table 1. Inhibition constants of inhibitors assayed against PTP1B as described in the Experimental section

	$K_i \pm$ S.D. (μM)
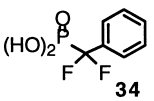 **34**	2,500 ± 120
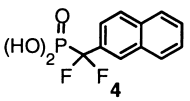 **4**	179 ± 25
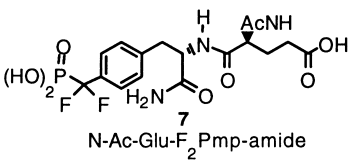 **7** N-Ac-Glu-F_2Pmp-amide	2.0 ± 0.14
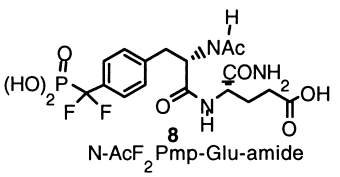 **8** N-AcF_2Pmp-Glu-amide	43.4 ± 2.2
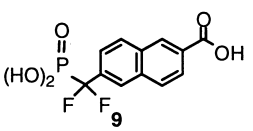 **9**	22.2 ± 1.1
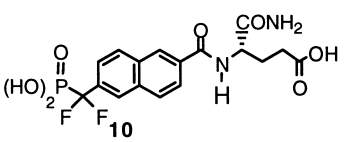 **10**	12.4 ± 0.9
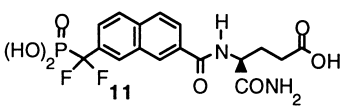 **11**	25.0 ± 2.0

PTP1B have shown that K_m values for free pTyr or aryl phosphates are 3- to 4-orders of magnitude higher than the best peptide substrates, indicating that amino acid residues flanking the pTyr moiety are important for efficient PTP1B catalysis.[9] Furthermore, it has been shown that acidic residues located proximal to the amino side of the pTyr residue are important for substrate recognition.[15,24] The recently solved crystal structure of the active site Cys215 to Ser mutant of PTP1B complexed with D-A-D-E-pTyr-L-amide reveals the structural basis for the favorable effect of acidic residues.[16] There are specific interactions between the acidic side chains (at -1 and -2 positions) of the substrate and the basic residue, Arg47 of the enzyme. These results suggest that the binding of peptide substrate/inhibitor is a cooperative event that involves the recognition of both pTyr/F_2Pmp functional groups as well as the structural features surrounding residues.

For high affinity small molecule PTP1B inhibitors, additional molecular features are required beyond the simple arylmethyl difluorophosphonate structure. We have appended various acidic functionalities onto F_2Pmp (generating **7** and **8**) and the naphthyl difluoromethylphosphonate **4** (generating **9–11**) to allow extra binding interactions with residues outside the catalytic site, especially Arg47. Relative to α,α-difluorobenzyl phosphonic acid **34**, the dipeptide analogue Ac-Glu-F_2Pmp-amide (**7**) displayed a 1240-fold higher affinity toward PTP1B. This is remarkable, since the hexapeptide analogue Ac-Asp-Ala-Asp-Glu-F_2Pmp-amide is only 11-fold better than the dipeptide. In contrast, the affinity of the "reverse order" dipeptide analogue Ac-F_2Pmp-Glu-amide (**8**) is reduced by 22-fold in comparison with Ac-Glu-F_2Pmp-amide (**7**). Thus, it is most likely that the Glu side chain situated amino-terminal to F_2Pmp in **7** would be able to interact with the side chain of Arg47, while the Glu side chain situated carboxy-terminal to F_2Pmp in **8** would not be able to make the same interaction as favorably. This indicates that directionality is important for substrate/inhibitor recognition by PTP1B, even for peptides as small as two amino acids.

Analogue **9** mimics a ring-constrained version of F_2Pmp (**2**). An eightfold enhancement in potency was observed for analogue **9** relative to the parent naphthyl difluoromethyl phosphonate **4**. Conceptually similar naphthalene bis-difluorophosphonates have also recently been reported to exhibit potent PTP1B inhibition.[25] Since the carboxyl group in **9** would not be expected to make direct interaction with the side chain of Arg47, the increased binding may arise from the interactions of the carboxylate with other residues in PTP1B or with Arg47 through bridged water molecules. Because **9** lacks the amino group found in F_2Pmp, coupling of **9** with a Glu

residue could not occur in a manner similar to that seen in dipeptide **7**. Instead the "pseudodipeptide" **10** was prepared in which the Glu residue effectively becomes situated at the carboxy-terminal side of the naphthyl difluoromethylphosphonate **4**, similar to the "reverse order" dipeptide **8**. Because the exact interaction of **10** with PTP1B could not be predicted with certainty, the isomeric naphthyl difluoromethyl phosphonate-containing dipeptide mimetic **11** was also prepared to introduce variation in the orientation of the acidic side chain relative to the naphthyl ring. As shown in Table 1, compound **10** exhibited a K_i value of 12.4 μM, which was twofold more potent than **11**. Since the parent naphthyl difluoromethylphosphonate **4** is 14-fold more potent than α,α-difluorobenzyl phosphonic acid **34**, the fact that compound **10** is sixfold less potent than **7** suggests that interaction of the Glu side chain in **10** with Arg47 may be less than optimal. Since molecular modelling predictions indicate that interaction of the inhibitors side chain carboxyl with the Arg47 guanidino group should readily occur, it was only logical to actually prepare and test the compound. That the binding affinity of **10** turned out to be lower than would be expected based on optimum interaction with the Arg47 guanidino group, may be rationalized as resulting from competition between the carboxyl and solvent for interaction with the guanidino group as suggested by dynamics simulations. This provides an example where actual experimental fact serves to place perspective on modelling predictions.

Experimental

Biological evaluation

Recombinant human PTP1B. The cDNA encoding the catalytic domain of human PTP1B (amino acids 1 to 321) was obtained using the polymerase chain reaction (PCR) from a human fetal brain cDNA library (Stratagene). The PCR primers used were 5′-AGCTGGATCCATATGG AGATGGAAAAGGAGTT (encoding both a *BamH*I and a *Nde*I site), and 3′-ACGCGAATTCTTAATTGTGTGGCTCCAGGATTCG (encoding an *Eco*RI site). The PCR product was digested with *BamH*I and *Eco*RI and subcloned into a pUC118 vector. The PTP1B coding sequence was confirmed by DNA sequencing. The coding region for PTP1B was then cut from pUC118-PTP1B with *BamH*I and *Eco*RI and ligated to the corresponding sites of plasmid pT7-7. The PTP1B coding sequence was placed in frame downstream of the phage T7 RNA polymerase promoter at the *Nde*I site of pT7-7 to provide the translational initiation at Met 1 of PTP1B. The resulting plasmid pT7-7/PTP1B was used to transform *E. coli* BL21(DE3). An overnight culture of BL2(DE3) cells with the pT7-7 expression vector containing the mutant PTP1B was diluted 1:100 into 1 L of 2×YT medium containing 100 g/mL ampicillin. The culture was grown at 37 °C until absorbance at 600 nm reached 0.6, at which point the cells were induced with 0.4 mM isopropyl fl-D-thiogalatoside for 6 h. The cells were harvested by centrifugation and stored at −20 °C. The frozen cell pellet was thawed at room temperature and resuspended in 30 mL of ice-cold buffer A (100 mM 2-(4-morpholino)-ethane sulfonic acid, pH 6.5, 1 mM DTT) and lysed by two passes through a French press at 1300 psi. All of the following steps were then carried out at 4 °C. The lysate was centrifuged at 15,000 rpm (Dupont SS-34 rotor) for 30 min. The supernatant was incubated with 50 mL of CM-Sephadex C50 equilibrated with buffer A and shaken gently for 40 min. The resin was washed three times with the same volume of buffer A, loaded onto a column and washed again with 10 bed volumes of buffer A. The protein was then eluted from the column by a linear gradient from 0 to 0.5 M NaCl in 200 L of buffer A. The positions of the peak fractions were assessed by Coomassie Blue staining of SDS-PAGE. Peak fractions which contain homogeneous PTP1B were combined into a final pool of protein, which was then concentrated to 30 mg/mL.

Phosphatase assay. The PTP1B phosphatase activity was assayed at 30 °C in a reaction mixture (0.2 mL) containing appropriate concentrations of *p*-nitrophenylphosphate (*p*NPP) as substrate. The buffer used was pH 7.0, 50 mM 3,3-dimethylglutarate, 1 mM EDTA. The ionic strength of the solution was kept at 0.15 M using NaCl. The reaction was initiated by addition of enzyme and quenched after 2–3 min by addition of 1 mL of 1 N NaOH. The nonenzymatic hydrolysis of the substrate was corrected by measuring the control without the addition of enzyme. The amount of product *p*-nitrophenol was determined from the absorbance at 405 nm using a molar extinction coefficient of 18,000 $M^{-1}\,cm^{-1}$. Steady state kinetic parameters were evaluated by fitting directly the v versus [S] data to the Michaelis–Menten equation using KINETASYST (IntelliKinetics, State College, PA, USA).

Inhibition constant (K_i) determination. Inhibition constants for the small PTP inhibitors was determined for PTP1B in the following manner. The initial rate at eight different *p*NPP concentrations (0.2–5 K_m) was measured at three different fixed inhibitor concentrations.[26] The inhibition constant and inhibition pattern were evaluated using a direct curve-fitting program KINETASYST.

Molecular modelling

All molecular modelling was performed using Insight II (version 95.5)[27] on Silicon Graphics Indigo2 R10000

work stations running IRIX (version 6.2), with molecular dynamics simulations and energy minimizations being conducted using the Discover 3 module. Cff91 force field and charge templates were employed, as were cell-multipole methods, for calculation of nonbonded interactions.[28–30] The previously determined X-ray structures of PTP1B in complex with the phosphopeptide ligand, Ac-D-E-pY-L (**35**)[16] or with the naphthalene diflourophosphonate **4**,[14] provided the structural basis for initial alignment of inhibitors examined in this study. Specifically, the initial structure of PTP1B in complex with **7** was constructed starting from the reported PTP1B·**35**, by substituting the phosphate ester oxygen bridge with difluoromethylene unit, replacing the Ac-Asp portion with an acetyl group and deleting the Leu residue, leaving the C-terminal primary tyrosylamide. Similarly, the initial PTP1B·**8** complex was obtained by changing the configuration of the α-carbon of PTP1B·**7**. Starting PTP1B·**10** and PTP1B·**11** complexes were derived from the published PTP1B·**4** structure by appending appropriate functionality to the naphthyldifluorophosphonate ring. Hydrogens were added to heavy atoms according to their hybridization, with protonation states of ligand and protein residues being assigned at pH 7, unless otherwise stated. Under these conditions, the phosphate group is present in its di-deprotonated form. Each complex was solvated with approximately 1500 TIP3P waters contained within a $27\approx$ radius sphere centered at the site of phosphate or phosphonate attachment to the aryl ring.

Since our primary goal was to achieve an understanding of the interactions between PTP1B and the ligands, molecular dynamics simulations were focused on the binding region. In order to avoid boundary effects, boundary regions of PTP1B complexes were excluded from simulations. Based on the X-ray structures of PTP1B both free and in complex with **4** and **35**, it is apparent that upon ligand binding, the enzyme does not undergo significant conformational change outside the binding region. Based on these considerations, each inhibitor–ligand complex was divided into both moveable and fixed regions. Moveable regions included the ligand itself as well as all protein residues and water molecules (approximately 380) within $20\approx$ of the ligand. The remainder of the system was fixed, meaning that atoms participated in interactions, but did not move. In this fashion, computational speed was significantly enhanced, while focusing attention on the binding region. For each study, a sequential stepwise process of minimization and simulation was performed, consisting of the following: (1) 1000 steps of minimization using a conjugate-gradient method (Polak-Ribiere); (2) 10 ps of molecular dynamics simulations at T = 598 K; (3) 20 ps of molecular dynamics simulations at T = 498 K; (4) 30 ps of molecular dynamics simulations at T = 398 K; (5) 40 ps of molecular dynamics simulations at T = 348 K; (6) 100 ps of molecular dynamics simulations at T = 298 K. The first round of minimizations was intended to eliminate high energy overlapping resulting from initial complex construction, while the subsequent four rounds of dynamics simulations were conducted as annealing processes to overcome potential energy barriers between different binding modes, thereby achieving a low energy state for the system. The final simulation at 298 K was undertaken to achieve an equilibrated distribution of structural and energetic properties for the enzyme–ligand complex.

General synthetic methods

Melting points were determined on a Mel Temp II melting point apparatus and are uncorrected. Elemental analyses were obtained from Atlantic Microlab, Norcross, GA, and fast atom bombardment mass spectra (FABMS) were acquired with a VG Analytical 7070E mass spectrometer under the control of a VG 2035 data system. ^{1}H NMR data were obtained on Bruker AC250 (250 MHz) or if indicated, AMX500 (500 MHz) instruments and are reported in ppm relative to TMS and referenced to the solvent in which they were run. Infrared spectral were acquired on a Perkin-Elmer 1600 series FTIR instrument. Solvent was removed by rotary evaporation under reduced pressure and silica gel chromatography was performed using Merck silica gel 60 with a particle size of 40–63 μ. Anhydrous solvents were obtained commercially and used without further drying. Preparative HPLC were conducted using a Vydac preparative C_{18} peptide and protein column. Dipeptides **7** and **8** were prepared by solid-phase techniques.

2,6-Naphthalenedicarboxylic acid monobenzyl ester (13). A suspension of 2,6-naphthalendicarboxylic acid **12** (10.8 g, 50.0 mmol) in anhydrous DMF (500 mL) with 1,8-diazabicyclo[5.4.0]undec-7-ene (DBU; 7.5 mL, 50 mmol) was heated to near boiling, then stirred at room temperature. To the resulting fine suspension was added benzyl bromide (6 mL, 50 mmol), portionwise over 10 min, giving a solution. After three days the solution was diluted with 0.5 N HCl/brine (1 L), extracted with EtOAc and the combined organic extracts were washed with H_2O, dried ($MgSO_4$) and taken to dryness to yield an off-white solid. The solid was suspended in ether, diluted with an equal volume of petroleum ether, then collected, washed with petroleum ether, and dried, yielding a white solid (8.11 g). The solid was dissolved in EtOAc (50 mL) and NEt_3 (4 mL, 29 mmol) was added with slight warming to effect total dissolution of all solid. This was applied to a 6.5-cm sintered glass funnel containing 200 mL of a 1/1 mixture of 5–25 μ silica and 63–200 mesh basic alumina oxide. Initial elution with EtOAc provided 2,6-naphthalenedicarboxylic acid dibenzyl

ester. Subsequent elution with EtOAc/formic acid (99/1) brought desired product. Evaporation of solvent and suspension of the resulting solid in petroleum ether, followed by collection and drying of solid gave pure **13** as white crystals (2.62 g, 17%): mp 242–243 °C (dec); ^{1}H NMR (DMSO-d_6) δ 8.75 (s, 1H), 8.69 (s, 1H), 8.21–8.30 (m, 2H), 8.12–8.03 (m, 2H), 7.56–7.38 (m, 5H), 5.45 (s, 2H). Analysis ($C_{19}H_{14}O_4 \cdot {}^1/_8H_2O$): C, H.

6-Hydroxymethyl-2-naphthalenedicarboxylic acid benzyl ester (14). To a suspension of **13** (2.89 g, 9.4 mmol) in anhydrous THF (50 mL) under argon at room temperature, was added 1.0 M BH_3·THF (11.3 mL). The resulting light brown solution was stirred overnight, then partitioned between brine (200 mL) and EtOAc (3×75 mL), dried ($MgSO_4$), and taken to dryness to yield a white crystalline solid. Trituration with petroleum ether and drying provided **14** sufficiently pure for further use (2.31 g, 84%), mp 88–94 °C. An analytical sample provided mp 98–99 °C: ^{1}H NMR (DMSO-d_6) δ 8.65 (s, 1H), 8.13–7.93 (m, 4H), 7.59–7.38 (m, 6H), 5.48–5.43 (m, 2H), 4.71 (d, 2H, J = 5.6 Hz). Analysis ($C_{19}H_{16}O_3$): C, H.

6-Formyl-2-naphthalenedicarboxylic acid benzyl ester (15). A mixture of **14** (2.0 g, 6.8 mmol) and activated MnO_2 (5.91 g, 68 mmol) in toluene (75 mL) was stirred at reflux under argon (30 min), then filtered through Celite. The Celite was washed with EtOAc and combined organics taken to dryness to yield product **15** as an oil which crystallized (2.0 g, 100%). An analytical sample was obtained by recrystallization from ether/petroleum ether, mp 75.5–78.5 °C: ^{1}H NMR (DMSO-d_6) δ 10.21 (s, 1H), 8.77 (s, 1H), 8.68 (s, 1H), 8.34–8.29 (m, 2H), 8.04 (dd, 1H, J = 1.5, 8.6 Hz), 7.98 (dd, 1H, J = 1.5, 8.6 Hz), 7.58–7.39 (m, 5H), 5.45 (s, 2H). Analysis ($C_{19}H_{14}O_3$): C, H.

Di-(*tert*-butyl) [(6-(benzyloxycarbonyl)naphth-2-yl)hydroxymethyl]phosphonate (16). A suspension of **15** (580 mg, 2.0 mmol) in di-(*tert*-butyl) phosphite (776 mg, 4.0 mmol) was warmed at 75 °C under argon. To the resulting solution was added basic Woelm aluminum oxide (4.0 g) and the mixture then maintained at 75 °C (1 h). The aluminum oxide was then extracted well with EtOAc/MeOH (1/1) and the combined extracts taken to dryness to yield a light yellow syrup. Silica gel chromatographic purification ($CHCl_3$) first eluted starting **15** (213 mg) followed by product **16**, which was obtained as a white crystalline solid (560 mg, 91% based on recovered starting material), mp 154 °C soften, 162–165 °C: ^{1}H NMR (DMSO-d_6) δ 8.65 (s, 1H), 8.10 (d, 1H J = 8.6 Hz), 8.50–7.97 (m, 3H), 7.68 (d, J = 8.6 Hz), 7.56–7.50 (m, 2H), 7.48–7.35 (m, 3H), 6.2–6.1 (m, 1H), 5.43 (s, 2H), 4.95–4.85 (m, 1H), 1.36 (s, 9H), 1.33 (s, 9H). Analysis ($C_{27}H_{33}O_6P \cdot 0.8H_2O$): C, H.

Di-(*tert*-butyl) [(6-(benzyloxycarbonyl)naphth-2-yl)difluoromethyl]phosphonate (18). To 5 mL of anhydrous CH_2Cl_2 in a dry 100 mL rb at −78 °C under argon was added oxalyl chloride, 2.0 M in CH_2Cl_2 (1.39 mL, 2.79 mmol). A solution of DMSO (394 L, 5.56 mmol) in anhydrous CH_2Cl_2 (3 mL) was then added, followed by a solution of **16** (674 mg, 1.39 mmol) in anhydrous CH_2Cl_2 (5 mL). After stirring at −78 °C (35 min) NEt_3 (1.40 g, 13.9 mmol) was added and stirring continued at −78 °C (10 min), then the reaction was then transferred to an ice bath and stirred at 0 °C (20 min). The mixture was partitioned between ice-cold 0.2 N HCl/brine (200 mL) and EtOAc (3×50 mL), dried ($MgSO_4$), then taken to dryness to provide ketophosphonate **17** as a yellow syrup in quantitative yield which was then fluorinated directly: ^{1}H NMR ($CDCl_3$) δ 9.05 (s, 1H), 8.58 (s, 1H), 8.17–7.92 (m, 4H), 7.47–7.29 (m, 5H), 5.38 (s, 2H), 1.50 (s, 18H).

The crude **17** was cooled to −78 °C then DAST (923 L, 1.13 g, 7 mmol) was added and the reaction flask swirled at room temperature until a solution formed. The reaction mixture was then stirred overnight on an ice bath which was allowed to come to ambient temperature gradually. The reaction mixture was cooled to −78 °C, diluted with $CHCl_3$ (50 mL) and shaken with ice-cold saturated $NaHCO_3$ (100 mL). The organic layer was combined with $CHCl_3$ back-extracts of the aqueous phase and washed with ice-cold saturated $NaHCO_3$ (100 mL), then dried ($MgSO_4$), and taken to dryness to yield a yellow syrup. Purification by silica gel chromatography (petroleum ether containing first 10%, then 30% EtOAc) provide pure **18** as light yellow crystals (390 mg, 59%), mp 91.5–92.5 °C: A sample was recrystallized for analysis (EtOAc/hexanes) mp 92–93 °C: ^{1}H NMR ($CDCl_3$) δ 8.60 (s, 1H), 8.11–8.04 (m, 2H), 7.95–7.87 (m, 2H), 7.67 (d, 1H, J = 8.6 Hz), 7.46–7.30 (m, 5H), 5.37 (s, 2H), 1.40 (s, 18H). Analysis ($C_{27}H_{31}O_5PF_2$): C, H.

Solid-phase synthesis of 10

To **18** (339 mg, 0.72 mmol) in THF (15 mL) at room temperature was added 0.2 N LiOH (10.8 mL) dropwise and the reaction mixture then stirred (3.5 h). The mixture was chilled, then partitioned between ice-cold 0.2 N HCl/brine (200 mL) and EtOAc (2×100 mL), dried ($MgSO_4$), then taken to dryness to yield crude **19** (222 mg, 74%): ^{1}H NMR (DMSO-d_6) δ 8.69 (s, 1H), 8.30–8.15 (m, 3H), 8.06 (dd, 1H, J = 1.5, 8.6 Hz), 7.69 (d, 1H, J = 8.6 Hz), 1.41 (s, 18 Hz). Solid-phase coupling of crude **19** was achieved directly using manual techniques. A total of 0.2 mequiv of *N*-Fmoc Rink amide resin (Bachem, 0.46 mequiv/g) was washed well with several 2 mL portions of *N*-methyl-2-pyrolidoinone (NMP), then the Fmoc amino protection was removed by treatment

with 20% piperidine in NMP (2 mL, 20 min). The deblocked resin was washed well with NMP (10×2 mL), then coupled overnight with a solution of active ester formed by reacting 0.5 mmol each of *N*-Fmoc-glutamic acid γ-*tert*-butyl ester, 1-hydroxybenzotriazole (HOBT), and 1,3-diisopropylcarbodiimide (DIPCDI) in NMP (2 mL, 10 min). The resin was washed with NMP (10×2 mL), and the amino Fmoc-protection was removed by treatment with 2 mL 20% piperidine in NMP (20 min). A solution of **19** (83 mg, 0.2 mmol) in NMP (2 mL) was activated by treatment with HOBT (27 mg, 0.2 mmol) and DIPCDI (31 L, 0.2 mmol) at room temperature (10 min), then coupled with the resin (4 h). The resin was washed (5×2 mL NMP; 5×2 mL CH_2Cl_2) and dried. A 50% portion of the dried resin was swollen with CH_2Cl_2 then cleaved with trifluoroacetic acid (TFA) containing 5% anisole (5 mL, 30 min). The resulting supernatant was taken to dryness, dissolved in acetonitrile/H_2O (1/1), and purified twice by HPLC (retention time, 10.2 min; linear gradient 0–50% B over 30 min) to provide **10** as a white solid (19 mg, 44%): ^{1}H NMR (D_2O) δ 8.28 (brs, 1H), 8.08 (s, 1H), 7.99 (d, 1H, J=8.6 Hz), 7.98 (d, 1H, J=8.6 Hz), 7.75 (dd, 1H, J=8.6, 1.8 Hz), 7.64 (d, 1H, J=8.6 Hz), 4.45 (m, 1H), 2.49 (m, 2H), 2.1 (m, 2H); FABMS (−VE, glycerol matrix) m/z=429.059 (calcd M-H, 429.066). Analysis ($C_{17}H_{17}N_2O_7PF_2 \cdot H_2O$): C, H, N.

2,7-Dihydroxynaphthalene ditriflate (21). To a mixture of 2,7-dihydroxynaphthalene **20** (13.5 g, 84.4 mmol), 2,6-lutidine (19.9 g, 186 mmol) and DMAP (2.06 g, 17 mmol) in CH_2Cl_2 (140 mL) and THF (140 mL) at −78 °C was added Tf_2O (50 g, 177 mmol) dropwise over 30 min. The reaction mixture was stirred first at −78 °C (2 h), then at 0 °C (5 h), and then carefully quenched with saturated $NaHCO_3$ (250 mL). It was extracted with CH_2Cl_2 (3×200 mL), washed with brine (2×50 mL), dried (Na_2SO_4) and taken to dryness to provide crude product which was purified by silica-gel chromatography (hexane/EtOAc, 4/1) to afford **21** as a white solid (26.4 g, 74%). An analytical sample was obtained by crystallization from hexane/EtOAc (20/1) mp 61.5–62.5 °C: ^{1}H NMR ($CDCl_3$) δ 7.99 (2H, d, J=9.1 Hz), 7.8 (2H, d, J=2.3 Hz), 7.47 (2H, dd, J=9.1, 2.3 Hz). Analysis ($C_{12}H_6F_6O_6S_2$): C, H.

2,7-Naphthalenedicarboxylic acid dimethyl ester (22). A flask containing a mixture of **21** (5.45 g, 12.9 mmol), $Pd(OAc)_2$ (352 mg, 1.57 mmol,), and $Ph_2P(CH_2)_3PPh_2$ (648 mg, 1.57 mmol) was degassed and recharged three times with CO: then MeOH (12.6 g, 393 mmol), DMSO (52 mL), and NEt_3 (4.77 g, 47.1 mmol), were successively added. This mixture was kept at 70 °C (5 h), then cooled to room temperature, and treated with brine (70 mL), extracted with EtOAc (3×80 mL), washed with brine (2×10 mL), dried (Na_2SO_4), and taken to dryness to provide crude product. Purification by silica-gel chromatography (hexane/EtOAc, 95/5) afforded **22** as a white solid (2.64 g, 84%): mp 136.5–137.5 °C; ^{1}H NMR ($CDCl_3$) δ 8.68 (2H, brs), 8.16 (2H, dd, J=8.6, 1.3 Hz), 7.91 (2H, d, J=8.6 Hz), 3.99 (6H, s). Analysis ($C_{14}H_{12}O_4$): C, H.

2,7-Di(hydroxymethyl)naphthalene (23). To a suspension of $LiAlH_4$ (3.28 g, 86.4 mmol) in THF (52 mL) was added **22** (2.64 g, 10.8 mmol) and the reaction mixture stirred at room temperature (3 h), then quenched with 1 N HCl (30 mL) at 0 °C. The mixture was then extracted with ether (3×50 mL), washed with brine (2×15 mL), dried (Na_2SO_4), and taken to dryness to yield crude product. Purification by silica-gel chromatography (CH2Cl$_2$/MeOH, 98/2) yielded **23** as a white solid (1.2 g, 59%): mp 158–160 °C; ^{1}H NMR ($CDCl_3$) δ 7.83 (2H, d, J=8.3 Hz), 7.79 (2H, brs), 7.67 (2H, dd, J=8.3, 1.3 Hz), 4.85 (4H, d, J=3.9 Hz), 1.54 (2H, s). Analysis ($C_{12}H_{12}O_2$): C, H.

2,7-Di(hydroxymethyl)naphthalene mono-*tert*-butyldimethylsilyl ether (24). To a solution of compound **23** (2.33 g, 12.4 mmol) in THF (62 mL) at 0 °C was added dropwise $LiN(TMS)_2$ (12.4 mL, 1.0 M in THF). After 30 min, DMAP and TBDMSCl was added in one portion and the mixture stirred at room temperature (overnight), then quenched with 0.2 N HCl (30 mL), extracted with EtOAc (3×50 mL), washed with brine (2×30 mL), dried (Na_2SO_4), and taken to dryness to yield crude product. Purification by silica gel chromatography (hexane/EtOAc, 4/1) provided **24** as a white solid (1.7 g, 45%): mp 41.5–43.5 °C; ^{1}H NMR ($CDCl_3$) δ 7.82–7.76 (4H, m), 7.42 (2H, dt, J=1.6 Hz, 8.2 Hz), 5.28 (2H, s), 5.25 (2H, d, J=5.8 Hz), 1.54 (1H, s), 0.95 (9H, s), 0.11 (6H, s). Analysis ($C_{18}H_{26}SiO_2$) C, H.

7-(*tert*-Butyldimethylsilyoxymethyl)naphthalene-2-carboxaldehyde (25). To a solution of **24** (7.01 g, 23.3 mmol) in toluene (200 mL) was added MnO_2 (20.0 g, 230 mmol) at room temperature. The mixture was heated to reflux (40 min), then brought to room temperature and filtered. The filtrate was taken to dryness to provide crude product, which was purified by silica gel flash chromatography (hexane/EtOAc, 4/1) to provide **25** as a white solid (5.34 g, 77%): mp 38–39.5 °C; ^{1}H NMR ($CDCl_3$) δ 10.83 (1H, s), 9.00 (1H, brs), 8.62–8.52 (4H, m), 8.26 (1H, dd, J=8.6, 1.5 Hz), 5.6 (2H, s), 1.66 (9H, s), 0.83 (6H, s). Analysis ($C_{18}H_{24}SiO_2$) C, H.

7-(*tert*-Butyldimethylsilyoxymethyl)naphthalene-2-carboxylic acid (26). To a mixture of **25** (5.55 g, 18.5 mmol), KH_2PO_4 (3.28 g, 24.1 mmol), 2-methyl-2-butene (3.25 g, 46.3 mmol), *t*-BuOH (92.5 mL), and H_2O (85 mL) at room temperature, was added $NaClO_2$ (2.18 g, 24.1 mmol) in one portion and the reaction mixture was

stirred at room temperature overnight. The *t*-BuOH was reduced in volume under reduced pressure, then the pH was adjusted to 5–6 by addition of 2 N HCl. The mixture was extracted with EtOAc (4×50 mL), washed with brine (2×20 mL), dried (Na_2SO_4), and taken to dryness to give crude product which, after purification by silica gel chromatography (hexane/EtOAc, 1/1) afforded **26** as a white solid (5.75 g, 98%): ^{1}H NMR ($CDCl_3$) δ 8.7 (1H, brs), 8.1 (1H, dd, J=9.1, 1.6 Hz), 7.92–7.84 (3H, m), 7.55 (1H, d, J=5.4 Hz), 4.89 (2H, s), 0.98 (9H, s), 0.14 (6H, s). Analysis ($C_{18}H_{24}SiO_3$) C, H.

7-(*tert*-Butyldimethylsilyoxymethyl)naphthalene-2-carboxylic acid benzyl ester (27). To a solution of **26** (852 mg, 2.7 mmol) in DMF (9 mL) was added DBU (534 mg, 3.51 mmol) and benzyl bromide (600 mg, 3.51 mmol) and the mixture stirred at room temperature (20 h). The mixture was quenched with 1 N HCl (4 mL), diluted with brine (10 mL), extracted with ether (3×50 mL), washed with brine (2×10 mL), dried (Na_2SO_4) and taken to dryness to yield crude product which was purified by silica-gel chromatography (hexane/EtOAc, 99/1) to provide **27** as a white solid (1.01 g, 92%): mp 50.5–52.0 °C; ^{1}H NMR ($CDCl_3$) δ 8.62 (1H, s), 8.06 (1H, dd, J=1.5, 8.5 Hz), 7.85 (3H, m), 7.41 (3H, m), 5.43 (2H, s), 4.90 (2H, s), 0.96 (9H, s), 0.13 (6H, s). Analysis ($C_{25}H_{30}SiO_3$) C, H.

7-(Hydroxymethyl)naphthalene-2-carboxylic acid benzyl ester (28). To a solution of **27** (6.66 g, 16.4 mmol) in THF (82 mL) was added tetrabutylammonium fluoride, 1.0 M in THF (21.3 mL, 21.3 mmol) and the mixture stirred at room temperature overnight, then quenched with brine (50 mL), extracted with $CHCl_3$ (3×70 mL), washed with brine (2×20 mL), (over Na_2SO_4) and taken to dryness. Purification by silica gel chromatography (hexane/EtOAc, 1/1) provided **28** as a white solid (4.44 g, 93%): mp 91.0–92.0 °C; ^{1}H NMR ($CDCl_3$) δ 8.62 (1H, s), 8.07 (1H, dd, J=8.6, 1.6 Hz), 7.9–7.82 (3H, m), 7.58 (1H, dd, J=8.6, 1.6 Hz), 7.5–7.34 (5H, m), 5.41 (2H, s), 4.88 (2H, brs). Analysis ($C_{19}H_{16}O_3$) C, H.

7-(Benzyloxycarbonyl)naphthalene-2-carboxaldehyde (29). To a suspension of pyridinium chlorochromate (634 mg, 2.94 mmol) in anhydrous CH_2Cl_2 (6 mL) was added a solution of **28** (286 mg, 0.98 mmol) in anhydrous CH_2Cl_2 (10 mL) via syringe. The mixture was stirred at room temperature (2 h), then filtered through a pad of celite, and the filter cake was washed with CH_2Cl_2 (2×10 mL). The combined organic was concentrated under reduced pressure and purified by silica gel flash column chromatograph, with hexane/EtOAc mixture from 9/1 to 4/1, to give **29** as a white solid (269 mg, 95%): mp 67–69 °C; ^{1}H NMR ($CDCl_3$) δ 10.17 (1H, s), 8.78 (1H, s), 8.43 (1H, s), 8.24 (1H, dd, J=1.7, 8.6 Hz), 7.92–7.88 (3H, m), 7.36–7.51 (5H, m), 5.44 (2H, s). Analysis ($C_{19}H_{14}O_3$): C, H.

Di-(*tert*-butyl) [(7-(benzyloxycarbonyl)naphth-2-yl)hydroxymethyl]phosphonate (30). To a solution of di-(*tert*-butyl) phosphite (194 mg, 1.00 mmol) in anhydrous THF (5 mL) was added a 1.0 M solution of lithium bis(-trimethylsilyl)amide in THF (1.0 mL, 1.0 mmol) at −78 °C under argon. After 30 min a solution of **29** (260 mg, 0.90 mmol) in THF (3 mL) was added and the mixture was stirred at −78 °C (2.5 h). The reaction was quenched by addition of 1 N HCl (1 mL) and extracted with $CHCl_3$ (3×10 mL). The combined organics were washed with brine (2×10 mL), dried (Na_2SO_4), and concentrated. Residue was purified by silica gel flash column chromatography (hexane/EtOAc, from 10/1 to 1/1) to yield **30** as a white solid (430 mg, 98%): ^{1}H NMR ($CDCl_3$) δ 1.40 (9H, s), 1.42 (9H, s), 3.38 (1H, brs), 8.62 (1H, s), 8.04 (2H, m), 7.84 (2H, m), 7.68 (1H, m), 7.48 (2H, m), 7.39 (3H, m), 5.41 (2H, s), 5.02 (1H, dd, J=10.5, 4.0 Hz). Analysis ($C_{27}H_{33}O_6P$): C, H.

Di-(*tert*-butyl) [(7-(benzyloxycarbonyl)naphth-2-yl)oxomethyl]phosphonate (31). To a solution of oxalyl chloride (228 mg, 1.8 mmol) in anhydrous CH_2Cl_2 (5 mL) was added DMSO (281 mg, 3.6 mmol) in CH_2Cl_2 (1 mL) at −78 °C under argon. The mixture was stirred (0.5 h) then a solution of **30** (428 mg, 0.9 mmol) in CH_2Cl_2 (5 mL) was added at −78 °C, and the mixture was stirred at −78 °C (1 h), then quenched with NEt_3 (911 mg, 9.0 mmol) and allowed to warm to room temperature. The mixture was then diluted with $CH2Cl_2$ (10 mL), washed with brine (3×10 mL), dried (Na_2SO_4), and concentrated. The crude product was purified by silica-gel chromatography (hexane/EtOAc, 4/1) to yield **31** as a clear thick oil (303 mg, 71%): ^{1}H NMR ($CDCl_3$) δ 9.19 (1H, s), 8.78 (1H, s), 8.24 (2H, m), 7.92 (2H, m), 7.35–7.50 (5H, m), 5.43 (2H, s), 1.55 (18H, s). Analysis ($C_{27}H_{31}PO_6 \cdot {}^3/_4H2O$): C, H.

Di-(*tert*-butyl) [(7-(benzyloxycarbonyl)naphth-2-yl)difluoromethyl]phosphonate (32). To a 25-mL flask containing **31** (320 mg, 0.66 mmol) at −78 °C under argon was added DAST (535 mg, 3.32 mmol) via syringe, then the reaction mixture was brought to 0 °C in an ice–water bath and allowed to come to room temperature with stirring overnight. The mixture was recooled to −78 °C, diluted with $CHCl_3$ (50 mL) and washed with 0.5 N NaOH (40 mL), then extracted with $CHCl_3$ (2×20 mL) and the combined organics washed with water (2×50 mL), dried (Na_2SO_4), and concentrated. Purification using a 1:1 mixture of 5–25 μ silica and 63–200 mesh basic alumina oxide (hexane/EtOAc, from 10/1 to 3/1) gave **32** as a solid (173 mg, 52%): mp 48.5–50.5 °C; ^{1}H NMR ($CDCl_3$) δ 8.69 (1H, s), 8.18 (1H, s), 8.16 (1H,

dd), 7.92 (2H, dd, $J=3.0$, 8.4 Hz), 7.77 (1H, d, $J=8.6$ Hz), 7.30–7.52 (5H, m), 5.42 (2H, s), 1.44 (18H, s). Analysis ($C_{27}H_{31}PO_5F_2 \cdot {}^3/_2H_2O$) C, H.

Solid-phase synthesis of 11. To an ice-cooled solution of **32** (160 mg, 0.317 mmol) in THF (8 mL) was added aqueous LiOH (0.2 N, 4.8 mL, 0.96 mmol) at 0 °C and the mixture was stirred at room temperature (3 h). The mixture was diluted with EtOAc (20 mL), washed with ice-cooled 0.2 N HCl/brine (20 mL) and the aqueous phase back-extracted with EtOAc (2×10 mL). The combined organics were washed with brine (35 mL) and dried (Na_2SO_4) and solvent removed under reduced pressure. The residue was taken up in a small amount of EtOAc, then diluted with hexane (1 mL) and solvent decanted off the resulting syrup, to yield di-(*tert*-butyl) [(7 - (carboxy)naphth - 2 - yl)difluoromethyl]phosphonate (**33**) which was dried under high vacuum and utilized directly for solid-phase synthesis. Coupling of **33** was achieved using manual solid-phase techniques. N^{α}-Fmoc-L-(O^{γ}-*tert*-butyl)glutamicamide Rink, prepared as indicated above (200 mg, 0.08 mmol) was washed with NMP (3×1 mL), then deblocked with 10% piperidine in NMP (1 mL, 20 min) and the resin washed with NMP (5×1 mL). Prederivatization of **33** (33 mg, 0.08 mmol) as its active ester was achieved by stirring with HOBT (11 mg, 0.08 mmol) in NMP (1 mL) in the presence of DIPCDI (11 mg, 0.08 mmol) at room temperature (10 min) prior to coupling overnight with the deblocked Glu-resin. The resulting resin was washed with NMP (5×1 mL) then CH_2Cl_2 (5×1 mL) and cleaved by treatment at room temperature with 1.6 mL of TFA/anisole (95/5; 30 min). The resin was then washed with CH_2Cl_2 (3×2 mL) and combined filtrates concentrated to yield crude product as a pink syrup, which was 79% pure by HPLC. This was dissolved in 2 mL of H_2O/MeCN (1/1) and purified by HPLC using a Vydac Peptide and Protein C_{18} reverse-phase column to yield **11** as a white powder (10.6 mg, 30%): ^{1}H NMR (D_2O) δ 8.45 (1H, s), 8.27 (1H, s), 8.09 (1H, s), 8.05 (1H, s), 7.89 (1H, d, $J=8.7$ Hz), 7.80 (d, 1H $J=8.3$ Hz), 4.60 (1H, q, $J=5.2$ Hz), 2.61 (2H, t, $J=7.2$ Hz), 2.28 (1H, m) 2.19 (1H, m); FABMS (*m*/*z*) 429 $[M-H]^-$. Analysis ($C_{17}H_{17}N_2O_7F_2P \cdot CF_3COOH \cdot {}^5/_2H_2O$): C, H.

Acknowledgements

Appreciation is expressed to Dr. James Kelley and Ms Pamela Russ of the LMC for mass spectral analysis. This work was partially supported by a Pilot Research Project Award to Z.-Y. Z. From the Howard Hughes Medical Institute—Research Resources for Medical Schools.

References and Notes

1. Barford, D. *Curr. Opin. Struct. Biol.* **1995**, *5*, 728.
2. Streuli, M. *Curr. Opin. Cell. Biol.* **1996**, *8*, 182.
3. Tonks, N. K.; Neel, B. G. *Cell* **1996**, *87*, 365.
4. Neel, B. G.; Tonks, N. K. *Curr. Opin. Cell. Biol.* **1997**, *9*, 193.
5. Jia, Z. C. *Biochem. Cell. Biol.* **1997**, *75*, 17.
6. Zhang, Z. Y. *Curr. Topics Cell. Reg.* **1997**, *35*, 21.
7. Levitzki, A.; Gazit, A. *Science* **1995**, *267*, 1782.
8. Burke, Jr. T. R.; Zhang, Z. Y. *Pept. Sci.*, in press.
9. Zhang, Z. Y.; Maclean, D.; Mcnamara, D. J.; Sawyer, T. K.; Dixon, J. E. *Biochemistry* **1994**, *33*, 2285.
10. Burke, Jr. T. R.; Smyth, M.; Nomizu, M.; Otaka, A.; Roller, P. P. *J. Org. Chem.* **1993**, *58*, 1336.
11. Smyth, M. S.; Burke, Jr. T. R.; *Tetrahedron Lett.* **1994**, *35*, 551.
12. Burke, Jr. T. R.; Kole, H. K.; Roller, P. P. *Biochem. Biophys. Res. Commun.* **1994**, *204*, 129.
13. Kole, H. K.; Smyth, M. S.; Russ, P. L.; Burke, Jr. T. R.; *Biochemical J.* **1995**, *311*, 1025.
14. Burke, Jr. T. R.; Ye, B.; Yan, X. J.; Wang, S. M.; Jia, Z. C.; Chen, L.; Zhang, Z. Y.; Barford, D. *Biochemistry* **1996**, *35*, 15989.
15. Zhang, Z. Y.; Thiemesefler, A. M.; Maclean, D.; Mcnamara, D. J.; Dobrusin, E. M.; Sawyer, T. K.; Dixon, J. E. *Proc. Natl. Acad. Sci. U. S. A.* **1993**, *90*, 4446.
16. Jia, Z. C.; Barford, D.; Flint, A. J.; Tonks, N. K. *Science* **1995**, *268*, 1754.
17. Smyth, M. S.; Ford, Jr. H.; Burke, Jr. T. R.; *Tetrahedron Lett.* **1992**, *33*, 4137.
18. Qiu, W. M.; Burton, D. J. *Tetrahedron Lett.* **1996**, *37*, 2745.
19. Blades, K.; Cockerill, G. S.; Easterfield, H. J.; Lequeux, T. P.; Percy, J. M. *Chem. Commun.* **1996**, 1615.
20. Taylor, S. D.; Dinaut, A. N.; Thadani, A. N.; Huang, Z. *Tetrahedron Lett.* **1996**, *37*, 8089.
21. Rink, H. *Tetrahedron Lett.* **1987**, *28*, 3787.
22. Gordeev, M. F.; Patel , D. V.; Barker, P. L.; Gordon, E. M. *Tetrahedron Lett.* **1994**, *35*, 7585.
23. Chen, L.; Wu, L.; Otaka, A.; Smyth, M. S.; Roller, P. P.; Burke, T. R., Jr.; Denhertog, J.; Zhang, Z. Y. *Biochem. Biophys. Res. Commun.* **1995**, *216*, 976.
24. Hippen, K. L.; Jakes, S.; Richards, J.; Jena, B. P.; Beck, B. L.; Tabatabai, L. B.; Ingebritsen, T. S. *Biochemistry* **1993**, *32*, 12405.
25. Wang, Q. P.; Huang, Z.; Ramachandran, C.; Dinaut, A. N.; Taylor, S. D. *Bioorg. Med. Chem. Lett.* **1998**, *8* 345.
26. Chen, L.; Montserat, J.; Lawrence, D. S.; Zhang, Z. Y. *Biochemistry* **1996**, *35*, 9349.
27. Insight II/Discover molecular modelling package by Molecular Simulations, Inc.
28. Greengard, L.; Rokhlin, V. I. *J. Comp Phys.* **1987**, *73*, 325.
29. Schmidt, K. E.; Lee, M. A. *J. Stat. Phys.* **1991**, *63*, 1223.
30. Ding, H. Q.; Darasawa, N.; Goddard, W. A., III. *J. Chem. Phys.* **1992**, *97*, 4309.